https://doi.org/10.5194/essd-2026-416
Preprint. Discussion started: 23 June 2026

Open Access Earth System Science Data Discussions

Historical Nansen Cast Temperature Profiles and the Ocean Heat Content Change since 19th Century

Viktor Gouretski, Lijing Cheng, Juan Du

Institute of Atmospheric Physics, Chinese Academy of Sciences, Beijing, China

Correspondence to: Viktor Gouretski (viktor.gouretski@posteo.de); Lijing Cheng (chenglij@mail.iap.ac.cn); Juan Du (dujuan10@mail.iap.ac.cn)

Abstract. The estimation of the ocean heat content (OHC) is based on the subsurface temperature observations which abundance, quality and accuracy changed over time following the development of oceanographic techniques and methods. The majority of the available global OHC time series begins in 1950s when the International Geophysical Year 1957-1958 (IGY) observational campaign resulted in a rapid improvement of the observational basis. However, a significant amount of subsurface temperature observations was accumulated during the period before the IGY. We perform a three-step quality control (QC) of the Nansen cast temperature profiles with the focus on the time period before 1970. The QC includes automated and manual control of temperature observations along with the quality control of temperature anomalies. The World Ocean Circulation Experiment/Argo Global Hydrographic climatology based on the high-quality temperature observations between 1990 and 2025 is used as the reference. To interpolate temperatures vertically we use a combination of the parabolic Reiniger and Ross (1966) method and the temperature anomaly method by Frankignoul (1981). The method is shown to result in a smaller interpolation error. Correction for depth bias in Nansen cast profiles are also suggested. The oldest temperature profiles from 1870s are treated separately, with the data from "Challenger" expedition used as reference. Finally, we estimate the OHC changes between 1870s and 2020s for six selected multi-year time periods. We find that for the layer 0-2000 m the OHC increase between 1920-1944 and 1945-1969 amounts to 30% of the total OHC increase between 1920-1944 and 2010-2025.

1 Introduction

Recognition of the crucial role of the global ocean for the Earth climate system and experimental evidences of the ocean warming highlighted the importance of the global archive of temperature profiles as it became clear that the OHC evolution can be estimated from the historical data (Levitus et al., 2005; Gourteski and Koltermann, 2007; Cheng et al., 2025; Pan et al., 2026). The majority of OHC time series based on subsurface hydrographic observations begins in the late 1950s, as the observational campaign during the IGY 1957-1958 for the first time permitted a quasi-global coverage of the global ocean with hydrographic observations.

It should be noted that a significant number of temperature and salinity profiles has been accumulated over the time period preceding the IGY. The "Challenger" expedition 1872-1876 marks the begin of the observational physical oceanography (Thomson and Murray, 1885; Roemmich et al., 2012). Guided by a group of scientists the expedition resulted in a large set of deep temperature profiles obtained with the accuracy and vertical resolution sufficient for the quantitative analysis of secular changes of the ocean thermal state. After the "Challenger" expedition several important improvements in oceanographic practice have been introduced. One is related to the further development of reversing

https://doi.org/10.5194/essd-2026-416
Preprint. Discussion started: 23 June 2026

Open Access Earth System Science Data Discussions

mercury thermometers (Negretti and Zambra, 1874) which soon replaced the minimum/maximum Six's thermometers used on the "Challenger" cruise (Austin and McConnel, 1980).

The other improvement is related to the thermometric method of thermometer depth estimation (Brennecke, 1921). The method found the first extensive application during the German Atlantic Expedition 1925-1927 (Wüst et al., 1932). The technique of taking water samples and measuring temperature at a number of depth levels is known under the name "Nansen cast" in commemoration of the Norwegian oceanographer Fritjoff Nansen who improved the method of serial hydrographic casts and developed the brass bottles (Nansen bottles) for taking water samples at depth levels (Helland-Hansen and Nansen, 1909; Nansen, 1906). Being gradually replaced by electronic profilers since late 1960s Nansen cast method remained in use until the beginning of 1990s as the main observational method on the ships of the former USSR - the country which contributed a significant part of all hydrographic hydrographic profiles between 1950s and 1990s. Since 1940 mechanical bathythermographs (MBT) (Spillhouse, 1938) began to contribute to the archive of temperature profiles. However the accuracy of MBT temperature measurements is much lower compared to that of Nansen casts and the maximum instrument depth is limited by 100-200 meters. The MBT data were found to be biased (Gouretski and Koltermann, 2007; Gouretski and Cheng, 2020).

Only a small number of the global-scale OHC estimates exists for the time period before 1950s. Zanna et al. (2018) produced OHC time series since 1871 based on global reconstructions, which link the OHC with the observed sea surface temperatures (Rayner et al., 2003) using Green's functions derived from the data assimilation experiments (Wunsch and Heimbach, 2007). Fu et al. (2025) provided the update of the above reconstructions. Roemmich et al. (2012) and Gebbie and Huybers (2019) used data from "Challenger" expedition to estimate OHC change after 1870s. Gouretski et al. (2012) provided estimates of the global temperature change between "Challenger" expedition and 1950s for the upper 400 m layer using in-situ hydrographic profiles.

In this study we describe the quality controlled and adjusted global archive of Nansen cast hydrographic profiles. Based on this dataset we access for the first time the change of the ocean heat content of the upper 2000 m layer over a 100 year time period between 1870s and 2020s.

2 Data

For the current analysis we use only Nansen cast temperature profiles obtained between 1873 and 2025, with the focus on the time period before 1970. The World Ocean Database (WOD) (Locarnini et al., 2023) (update as of August 2025) served as the main data source. The profiles from the WOD include *observed level data* from the Ocean Station Data (OSD) instrument type. A closer inspection of profiles suggests that some of them might represent vertically interpolated data, whereas another group of profiles may be a blend of data from both observed and interpolated levels. Unfortunately, in most cases no respective metadata exists regarding the possible application of the vertical interpolation. Apart from the WOD archive we used four temperature profile datasets which have been digitized using the published station logs. These include:

1) Temperature profiles of the British "HMS Challenger" 1872-1876 expedition (Thomson and Murray, 1889);

2) Temperature profiles from the cruises of the United States steamer "Tuscarora" in the North Pacific 1871-1874 (U. S. Hydrographic Office, 1874);

3) Temperature profiles from the German "Gazelle" 1874-1876 expedition (Hydrographisches Amt der Admiralität, 1888);

https://doi.org/10.5194/essd-2026-416
Preprint. Discussion started: 23 June 2026

Open Access Earth System Science Data Discussions

4) Temperature, salinity, and oxygen profiles from the German Atlantic Expedition obtained by the ship "Meteor" in 1925-1927 (Wüst et al, 1932). This dataset was used earlier for the estimation of secular changes in temperature and salinity in the South Atlantic Ocean (Gouretski et al., 2012).

All digitized profiles represent data at observed levels. The total number of temperature profiles between 1873 and 2025 retained for the analysis is 2,838,855, with 1,224,404 profiles for the time period before 1970. Quality controlled salinity and dissolved oxygen data are not used in the current analysis but accompany the temperature data when available. Automated quality control procedures for salinity and dissolved oxygen data are described by Gourteski (2018) and Gouretski et al. (2024).

2.1 Time and spatial distribution of profiles

The yearly number of profiles mirrors the development of the observational physical oceanography resulting in a rapid growth of the data volume (**Fig. 1a**). Two periods (1914-1918 and 1940-1947) which include the two World Wars are characterized by the drop of the number of observations at all levels. For all time periods the number of data rapidly decreases with depth. Before 1920s shallow profiles prevail, leaving the deep ocean essentially unsampled. Before 1920s a significant part of deep temperature measurements was obtained by the three expeditions in mid-1870s (**Fig. 1b**) mentioned in the previous section.

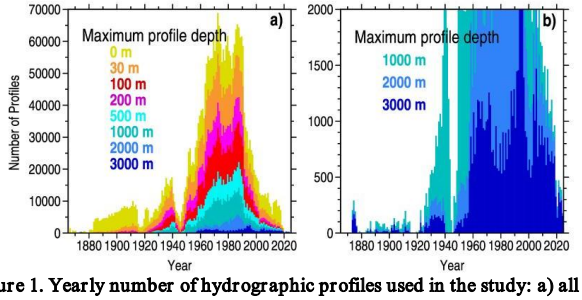

Figure 1. Yearly number of hydrographic profiles used in the study: a) all profiles; b) profiles deeper than 1000m.

The spatial distribution of profiles for selected time periods and for several maximum profile depths is given in **Fig. 2**. The two decade-long time period between 1950 and 1970, which includes the campaign of the International Geophysical Year (Chapman, 1955) is characterized by a quasi-global coverage even for the deep profiles. Before 1950 a relatively good spatial coverage (also with deep profiles) was achieved between 1920 and 1949, with the Atlantic Ocean exhibiting the most dense sampling. The sampling between 1900 and 1920 was almost completely confined to the Atlantic ocean. The largest data gaps are found in the remote central parts of the Pacific and Indian oceans. A coarse quasi-global array of ship tracks with subsurface temperature observations is available for the time period 1870-1900 with the most important contributions from the cruises by "HMS Challenger", "Gazelle", and "Tuscarora" in mid-1870s.

https://doi.org/10.5194/essd-2026-416
Preprint. Discussion started: 23 June 2026

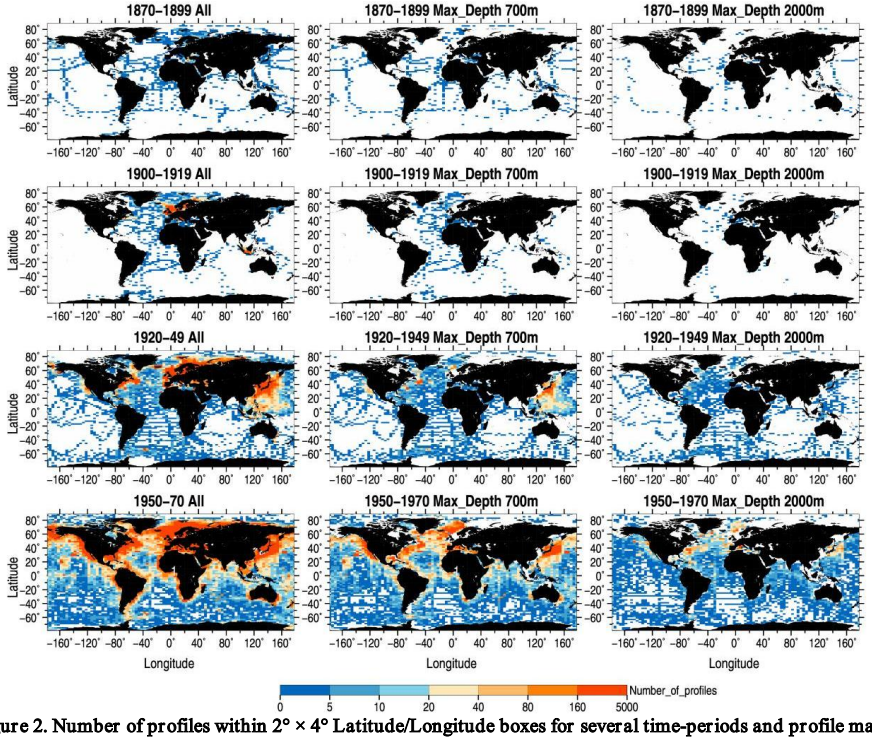

Figure 2. Number of profiles within 2° × 4° Latitude/Longitude boxes for several time-periods and profile maximum depths.

2.2 Characteristics of the vertical sampling

The accomplishing of Nansen casts becomes more difficult with the increasing cast depth. Deep casts require more wire, a larger number of bottles and thermometers, and a much longer cast time. For these reasons shallow casts are prevailing (**Fig. 3a**) with only 10 %, 5 % and 2.5 % of all casts being deeper than 1100 m, 1600 m, and 2500 m respectively. The dynamical load on sounding line (a hemp rope on the earliest cruises and a steel wire since the late 19th century) puts limitation on the maximum number of bottles which can be attached to the wire. Typically, not more than 10-12 bottles were used (Gould et al., 2013). Moroshkin (1951) reported about using up to 17 bottles during a cast. Therefore for deep hydrographic stations several casts had to be accomplished to provide a sufficient vertical resolution throughout the water column. **Fig. 3b** shows the histograms of the number of observed levels. The average number of observed levels versus cast depth (**Fig.3c**) indicates that on average about 23 observed levels are available for the profiles with the deepest level around 5000 m. The vertical gap between a pair of neighbor bottles typically increases with depth from one or several tenth of meter near the ocean surface to 500 m or more in the deep part of the profile (**Fig. 3d**).

Since Nansen casts take samples and measure temperature at a number of discrete levels, the choice of the levels is made to permit a finer vertical resolution in the more variable upper part of the water column. Shown in **Fig.4** is the sample depth histogram for the period 1920-1970. An disproportionately large number of observations comes from a limited number of levels corresponding to the so called 'standard depths' which were usually chosen as target depth levels for sampling. The set of standard depths was recommended in the hydrographic manuals (Borishanski, 1954; State Oceanographic Institute, 1977; U.S. Naval Oceanographic Office, 1968).

https://doi.org/10.5194/essd-2026-416
Preprint. Discussion started: 23 June 2026

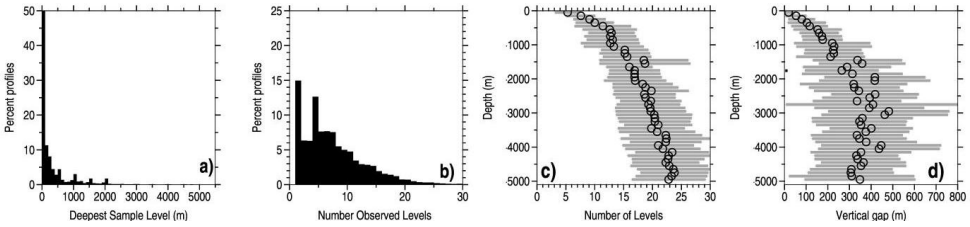

Fig.3. a) Deepest sample level histogram; b) number of observed levels histogram; c) mean number of observed levels versus cast depth; d) mean vertical gap size versus depth.

3 Data quality control

Imperfection and malfunctioning of instrumentation, especially in the early period, errors in reading temperature values, lack of the proper thermometer calibration, errors in sample depth lead to both random and systematic errors in temperature. The data used in the study undergone three steps of quality control: statistical automated quality control, manual quality control, and statistical quality control of temperature anomalies. The steps are described in sections 3.1, 3.2, and 6.2 respectively.

3.1 Statistical quality control

First, the original temperature profiles were put through the automated quality control procedure (Gouretski, 2018). The procedure consists of a suite of independent quality checks with parameter thresholds for each check based on statistical properties of the entire data population. Outlier diagnostics are shown in **Fig. 5a-c**. The overall percentage of the observed level temperature values identified as outliers is 4.2 %, with outliers found by 13 % of profiles. The outlier statistics suggest a gradual improvement of the data quality over time. The data before about 1920 are characterized by the highest percentages of outliers, which we attribute to the imperfectness of the observational technique.

3.2 Manual quality controlled

Secondly, temperature profiles obtained before 1970 were subjected to manual quality control. The data have been screened for remaining outliers in 507 5° × 20° Latitude/Longitude boxes (**Fig. S1**). Examples of quality-controlled temperature profiles for observed level data are shown in **Fig. S2** for selected boxes. The manual quality control identified 0.17% of all temperature observations as outliers with 0.85% profiles affected by the manual check (**Fig. 5d-f**)

4 Vertical interpolation of the observed level data

The choice of the interpolation method is important for historical profiles due to a sparse and uneven resolution over the water column. The originally crude vertical resolution further deteriorates due to the exclusion of observed levels during the quality control. As indicated by the **Fig. 3c** even the deepest profiles have on average about 23 observed levels. The distances between the observed levels (vertical gaps) increase with depth from typically 5-25 m near the surface to more than 300 m below about 1500 m (**Fig.3d**).

https://doi.org/10.5194/essd-2026-416
Preprint. Discussion started: 23 June 2026

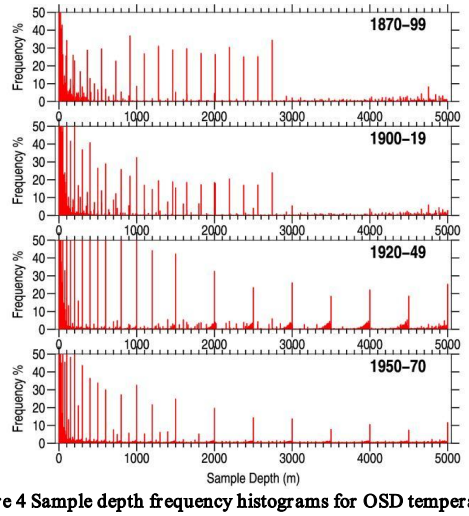

Figure 4 Sample depth frequency histograms for OSD temperature profiles for selected time periods.

To interpolate profiles vertically we use a combination of two methods: the parabolic Reiniger and Ross (1966) interpolation method (RR method), which uses only observed temperature and the climate anomaly method by Frankignoul (1981) (FR method) which interpolates deviations of individual temperature profiles from the respective climatology temperature profiles.

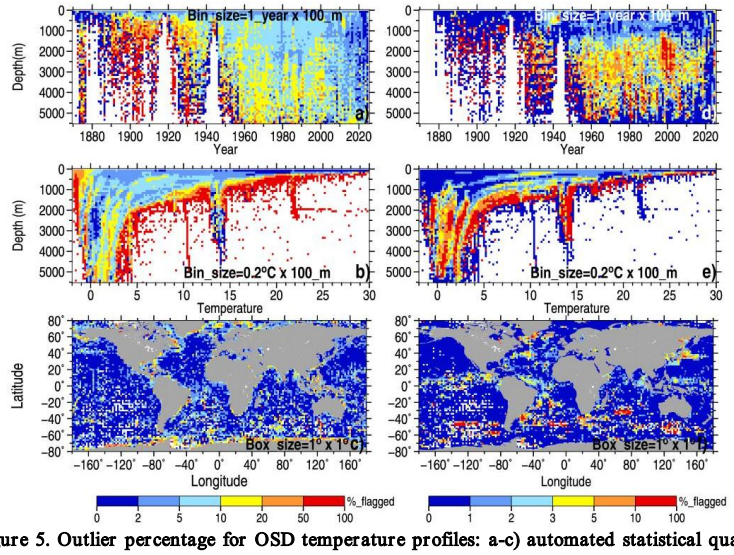

Figure 5. Outlier percentage for OSD temperature profiles: a-c) automated statistical quality control; d-f) manual quality control. Outlier percentage is shown for depth/year bins (a,d), depth/temperature bins (b,e), 1° × 1° latitude/longitude boxes (c, f).

4.1 Case of uneven distribution of observed levels over depth

https://doi.org/10.5194/essd-2026-416
Preprint. Discussion started: 23 June 2026

Open Access Earth System Science Data Discussions

The straightforward application of the RR method to observed level profiles was found to result in unrealistically large excursions on the interpolated temperature profile for a not-negligible number of profiles. Such cases typically occur when the observed levels are distributed extremely unevenly so that neighbor vertical gaps differ by more than an order of magnitude. Such profiles occur for instance when the entire temperature profile at a hydrographic station is composed of two or more hydrographic casts, each covering a part of the entire water column. When such profiles are merged together in the final station table the deepest observed depth of the shallower cast might be very close to the shallowest observed level of the deeper cast. In other cases small gaps may be due to the inclusion of the interpolated levels along with the observed levels in the resulting station table, or when big gaps on profiles appear due to the rejection of outliers. Since the interpolating polynomial must pass through each point of the original temperature profile unrealistic overshootings appear on the interpolated profile. **Fig. 6** shows several examples of such profiles. In some cases the overshooting amounts to several degrees. To avoid the overshooting the original profiles are checked for pairs of levels which are very close to each other before interpolation. Such pairs are then replaced by one level referred to the middle point and temperature is taken as the average of temperature at the two levels.

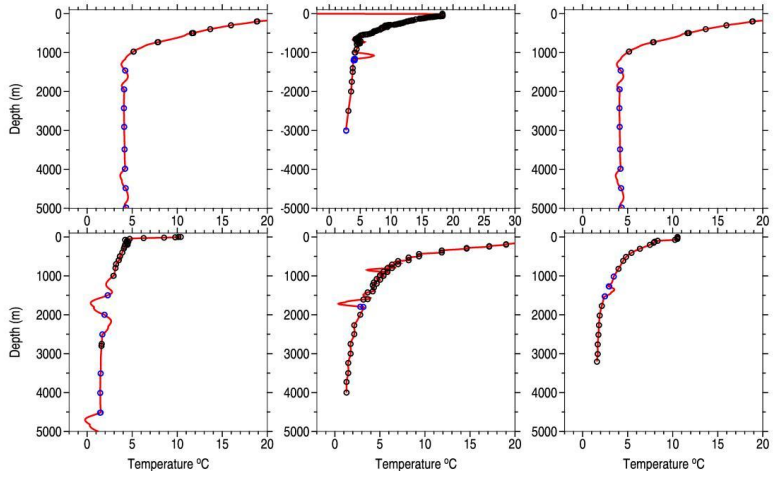

Figure 6. Examples of temperature profiles with uneven distribution of observed levels resulting in unrealistic overshooting of interpolation polynomials: observed levels (black circles), observed levels with a small distance to a neighbor level (blue circles), interpolated profile (red).

4.2 Dependence of interpolation error on distance between observed levels.

Due to non-linearity of temperature profiles interpolation over too big gaps might lead to big errors. In order to get a measure of interpolation error we used the climatology temperature profiles from the updated WAGHC climatology (Gouretski, 2018). The WAGHC gridded profiles give temperature values at 65 unevenly spaced levels between the surface and 6500 m. Each WAGHC profile was interpolated on 10-meter levels using the Reiniger-Ross interpolation. The vertical interpolation was then performed for a the resampled profile. Resampling was done by deleting a number of levels below the selected level so that the gap between the level under consideration and the next level below was increased iteratively. The root mean square difference between the interpolated values obtained using the full level profile and the profile with the reduced number of level gives a measure of interpolation error. **Fig. 7** shows the

https://doi.org/10.5194/essd-2026-416
Preprint. Discussion started: 23 June 2026

dependence of the interpolation error on the gap size and the depth of the upper gap boundary. The error increases with increasing gap size and decreases with increasing depth. The interpolation error in **Fig.7** corresponds to the error in the center of the gap.

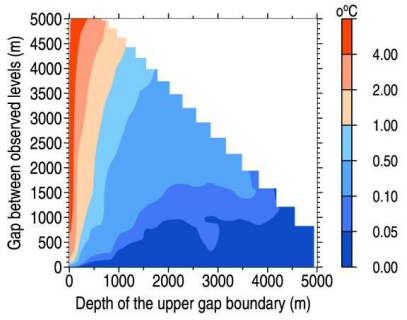

Figure 7. Dependence of interpolation error on the vertical gap size and the depth of the upper gap boundary.

4.3 Comparison of the Reiniger Ross interpolation method and the climate anomaly method

As suggested by the **Fig. 7** the interpolation error in RR method increases with the gap size. To reduce the error for big vertical gaps the climate anomaly method suggested by Frankignoul (1981) is used (FR method). In this method deviations of individual temperature profiles from the mean climatology are linearly interpolated over depth, and the interpolated value at a level is represented by the sum of the mean climatological temperature value and the interpolated anomaly. **Fig. 8** shows several selected observed profiles with big vertical gaps along with the respective interpolated profiles. For large gaps temperature differences between interpolated methods can exceed several degrees. The RR interpolation method in case of large gaps results in unrealistic temperature anomalies.

Figure 9 shows the dependence of the mean and mean absolute temperature error on gap size for RR and FR methods respectively. Whereas for small gaps both method produce very similar results, for large gaps the RR interpolation error is larger compared to FR method. For gaps larger than 300-500 m the mean absolute error for RR method can be up to factor 3-5 larger than the respective error for the FR method. We note that below 500 m the mean error for the FR method is close to zero even for the gaps larger than 500 m, whereas the RR method tends to result in a positive mean error increasing with the gap size. **Fig. 9** serves as the guidance to choose which method is to be used depending of the gap size and the depth layer. The results are summarized in the **Table 1** where threshold vertical gap size is given for distinct depth layers. If the actual gap for a pair of levels exceeds the threshold value the FR method is used to interpolate temperature between the two layers. For smaller gaps RR method is implemented.

The overall performance of the interpolation method described in the above sections is further illustrated by the temperature/depth histograms based on the observed and interpolated data respectively (**Fig.10**). To obtain these histograms the number for each temperature-depth bin is normalized by the number of observations in the most data abundant bin for each depth. A good agreement between the two histograms suggest the absence of spurious features in interpolated profiles.

https://doi.org/10.5194/essd-2026-416
Preprint. Discussion started: 23 June 2026

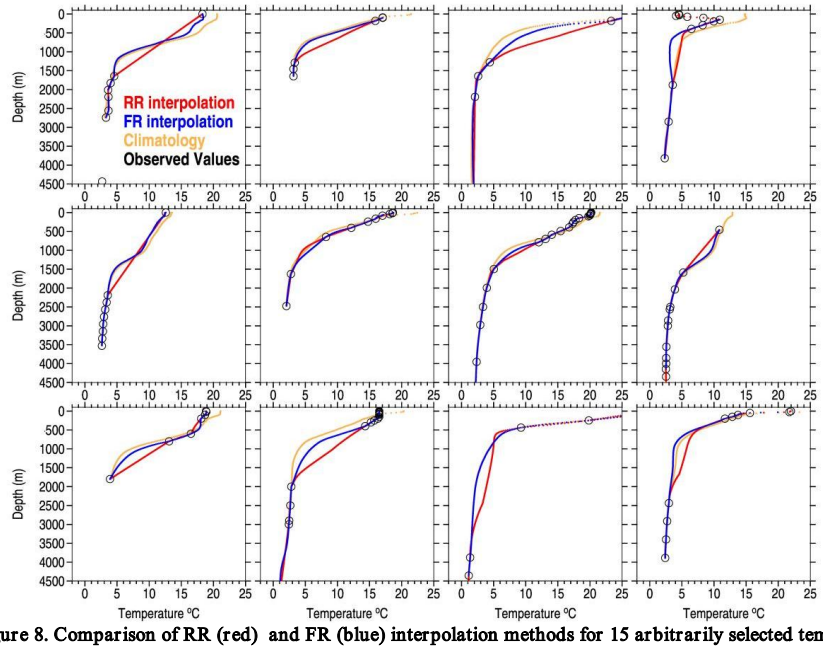

228 **Figure 8. Comparison of RR (red) and FR (blue) interpolation methods for 15 arbitrarily selected temperature profiles with**
229 **large vertical gaps. Observed level values are marked with black circles, WAGHC climatology temperature profiles are**
230 **shown in green.**

231

232 **Table 1. Threshold gap size for the choice on the interpolation method**

Depth Layer (m)	Threshold Gap Size (m)
0-100	100
100-200	100
200-300	100
300-500	150
500-1000	200
1000-1500	300
1500-2000	500
>2000	600

233

234

235

236

237

238

https://doi.org/10.5194/essd-2026-416
Preprint. Discussion started: 23 June 2026

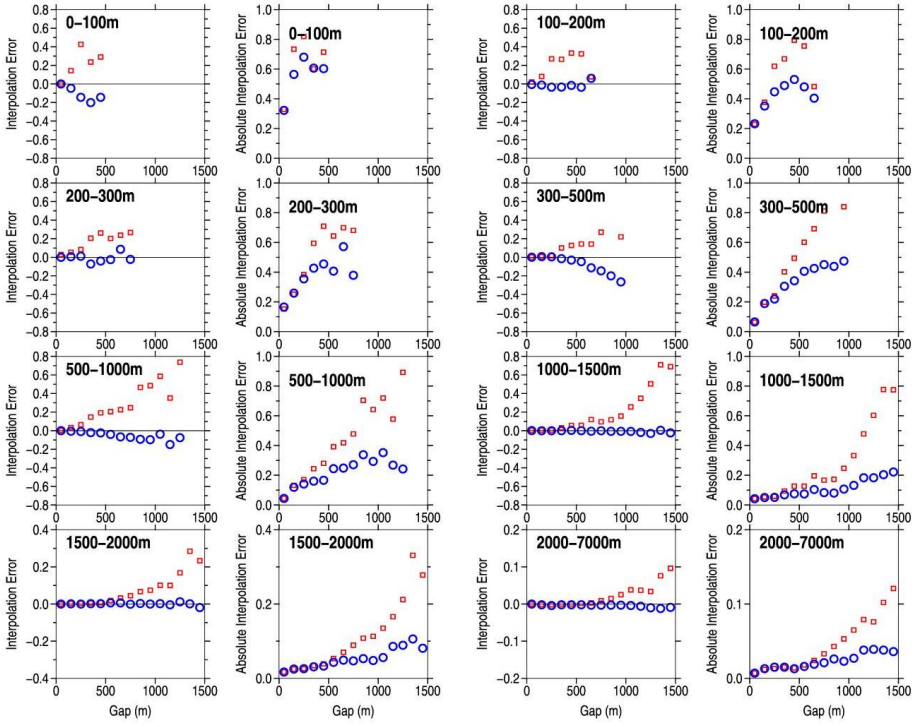

Figure 9. Mean and mean absolute error for interpolated temperature values obtained by means of RR method (red) and FR method (blue). Results are shown for eight selected depth layers.

5. Estimation of the Nansen cast depth bias

Only under ideal conditions the wire with attached Nansen bottles takes vertical position over the entire wire length. Because currents and wind cause ship drift during the occupation of the hydrographic station the wire deviates from the vertical so that the length of the wire paid out is greater than the actual depth at which the temperature was measured. Brennecke (1921) suggested to use paired pressure protected and pressure unprotected mercury in glass thermometers for the calculation of the actual bottle depth. The unprotected thermometer shows higher temperature compared to the protected one with the difference being dependent on hydrostatic pressure which can be re-calculated into depth. The method was first implemented during the German Antarctic Expedition 1911-1912, but the first full-scale implementation took place during the German Atlantic Expedition 1925-1927 (Wüst, 1932).

Unfortunately the thermometric method was not always implemented in oceanographic practice. Respectively, for a substantial number of Nansen casts the reported sample depths in reality represent target (standard) depth levels (see **Fig. 4)**. Typically, only several bottles of a hydrographic cast were equipped with paired thermometers. Since the pressure effect becomes noticeable only below a certain depth the paired thermometers were used at depths greater than several hundred meters. The potential depth bias for Nansen casts was investigated by Gouretski et al. (2022), who used collocated pairs of Nansen cast and temperature profiles from Conductivity/Temperature/Depth (CTD) profilers. Such collocated data are available only for the time period after 1970 since the introduction of CTDs. The Nansen casts were found to be biased in depth with the sample depth reported by station logs overestimating the actually reached depth. Gouretski et al. (2022) suggested corrections for depth bias and also pointed to another method of depth bias estimation,

https://doi.org/10.5194/essd-2026-416
Preprint. Discussion started: 23 June 2026

based on the analysis of the sample depth histogram. Here we imply this method to derive depth correction for old Nansen casts obtained before 1970. As illustrated by the **Fig. 4** the disproportionately large number of observations comes from a limited number of the so called standard levels which were chosen as target depth levels for sampling. The non-standard-depth levels can be linked to the profiles where thermometric method was used or where corrections were applied to account for the deviation of the wire from the vertical.

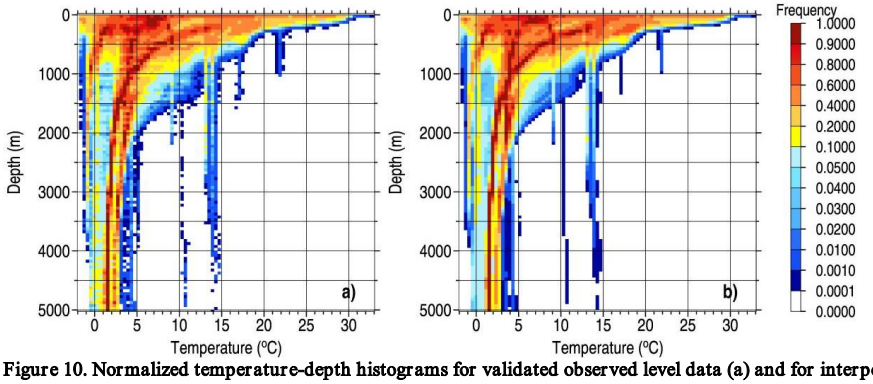

Figure 10. Normalized temperature-depth histograms for validated observed level data (a) and for interpolated data (b).

Figures 11a, b show frequency distribution of sampled depths around standard levels. These histograms were obtained after removing the standard levels and the subsequent smoothing using Gaussian kernel. For all 24 standard levels a shift of the maximum frequency depth (Z_{max}) relative to the respective standard level (Z_{stand}) can be seen. Using histograms depicted in **Fig.11a,b** the ratio R = (Z_{max})/(Z_{stand}) was calculated for each standard level (**Fig.11c**).Corrections are also given in **Table A1**. As indicated by **Fig.11c** reported sample depth slightly overestimate the actually reached depth. We note that Nansen cast bottle depths are reported in round meters imposing a limitation on the relative accuracy of the histogram method in the upper part of the water column.

Depth corrections were determined for the time period 1920-1970, for which no collocated CTD profiles are available. We note that depth corrections should not be applied for the profiles for which the usage of the thermometric method is confirmed by the respective metadata. The impact of the depth corrections on OHC estimates is discussed in section 8.5.

6 Calculation of temperature anomalies

One of the goals of the current study is to estimate changes in ocean heat content before the International Geophysical Year 1957-1958. Such estimation is based on temperature anomalies calculated relative to a base-line climatology.

6.1 WOCE-Argo Global Hydrographic Climatology – the reference ocean thermal state

The updated WOCE/Argo Global Hydrographic Climatology (WAGHC) (Gouretski, 2018) was used to calculate temperature anomalies. This climatology represents climate monthly values of temperature on a 0.5° square grid and is based on the extended set of Argo, bottle, and CTD profiles (status as of June 2024). The original version (Gouretski, 2018) included the latest temperature profiles from 2017. The climatology is based on 201,962 OSD profiles and 714,716 CTD profiles between 1990 and 2024, and 3,035,127 Argo profiles between 2001 and 2024. **Fig. S3** shows

https://doi.org/10.5194/essd-2026-416
Preprint. Discussion started: 23 June 2026

annual climate temperature field at selected levels. In a deviation to the widely used World Ocean Atlas climatologies (Garcia et al., 2018; Locarnini et al., 2023), the WAGHC climatology provides information about the median year of climatology temperature field (**Fig. S4),** which varies in the range 2014-2015 and 2003-2006 above and below the Argo maximum depth respectively.

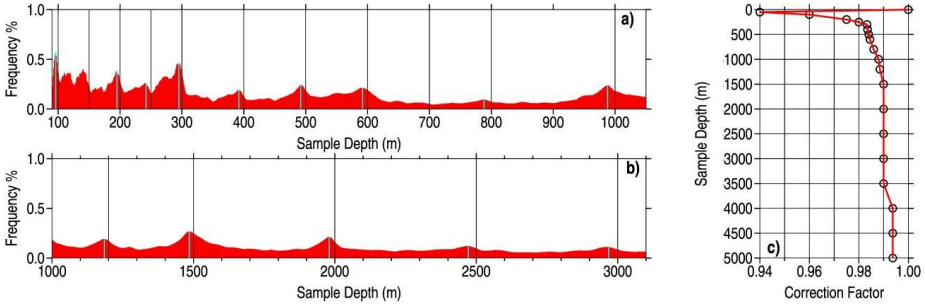

Figure 11. a, b) Smoothed sample depth histograms with deleted standard levels. Black vertical lines correspond to the standard depths, cyan bars denote maximum frequency. Differences between the standard depth and the depth of the respective local maximum frequency represent the depth bias; c) depth correction factor versus depth.

6.2 Temperature anomalies relative to the WAGHC climatology

For each observed temperature profile, climatology values are obtained by means of spatial interpolation of 0.5° × 0.5° climatology temperature fields. Above/below 200 m monthly/annual climatology fields were used respectively. The standard deviation of temperature anomalies within 2° × 4° latitude/longitude boxes (**Fig. S5**) reveals a well-known pattern with high variability areas confined to the western boundary current systems (Gulf Stream, Kuroshio, Agulhas, Malvinas), to the Antarctic Circumpolar current, and to the equatorial and tropical bands in the Pacific, Atlantic, and Indian oceans.

An additional quality control check is applied to individual temperature anomalies. First, the overall anomaly limits versus depth are calculated based on all temperature profiles. The mimimum/maximum anomaly limits are defined as the 1st and 99th quantiles respectively (**Fig. S6**). To arrive on local threshold at the geographical location (Lat, Lon) and at the depth level Z the overall thresholds are modified by the multiplicative factor $\sigma(x,y,z)/\sigma_{MEAN}(z)$, where $\sigma(x,y,z)$ is the anomaly standard deviation within the respective 2° × 4° Latitude/Longitude box, and σ_{MEAN} is the global mean of $\sigma_{MEAN}(z)$. **Fig. 12** shows outlier diagnostics for anomaly check. The check rejects 0.55% of all observations as outliers, with about 2.10% of profiles being affected.

https://doi.org/10.5194/essd-2026-416
Preprint. Discussion started: 23 June 2026

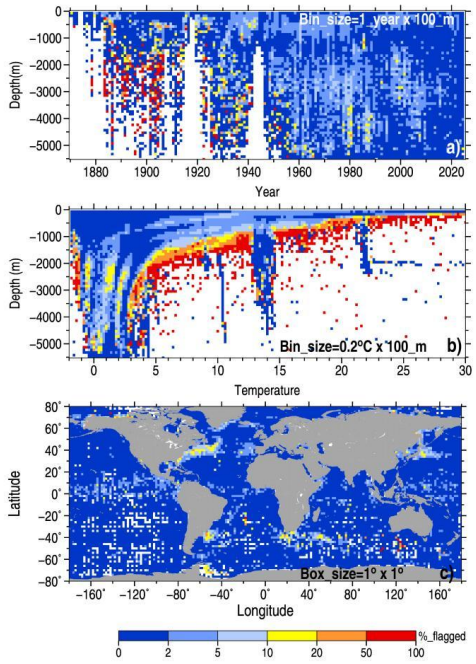

315 **Figure. 12. Outlier percentage for temperature anomalies: a) percentage in depth/year bins, b) depth/temperature bins, c) 1°**
316 **× 1° Latitude/Longitude boxes.**

317

318 **7 Adjustment of the oldest temperature profiles**

319 Whereas the first subsurface temperature measurements available in the WOD database date back to the cruises
320 from the end of 18th century, the voyage of "Challenger" (1873-1875) represents the first large-scale oceanographic
321 expedition with temperature measurements conducted by scientists. The comparison of the "Challenger" temperature
322 data with Argo-era temperatures revealed a profound warming of the global ocean along the entire track of the
323 expedition (Roemmich et al., 2012). Almost simultaneously with "Challenger" voyage two other major expeditions
324 were conducted by the German ship "Gazelle" (Hydrographisches Amt der Admiralität, 1888) and the US ship
325 "Tuscarora" (Belknap, 1874). Both cruises did not have scientists on board. The location of stations for all three
326 expeditions is shown in **Fig. 13a.** Analysis of temperature anomalies revealed significant systematic differences
327 between the expeditions, with the most pronounced disagreement found between "Challenger" and "Tuscarora"
328 temperatures. Because of a larger size, better vertical resolution, and a wider geographical scope of the "Challenger"
329 data, along with the fact that the measurements and their analysis being conducted under the scientific supervision, we
330 use the "Challenger" data as the reference to which temperatures from "Gazelle" and "Tuscarora" cruises are adjusted.
331 The choice of stations for comparison is defined by the maximum distance between profiles of 2000 km. For
332 "Challenger" and "Tuscarora" this area includes the majority of "Challenger" and "Tuscarora" stations in the North
333 Pacific , whereas for "Challenger"-"Gazelle" comparison profiles in all three oceans are used (**Fig. 13b, c**). Distribution
334 of point temperature anomalies over depth (**Fig. 13 d, e)** and binned anomalies **(Fig. 13f, g)** suggests a linear correlation
335 of anomaly differences between the expeditions. Linear regressions for binned anomalies below 500 m are: $\Delta T_{Gazelle}$ =
336 $0.223 - 9.195*10^{-5}$ Z; $\Delta T_{Tuscarora}$= $-0.130 - 1.358*10^{-4}$ Z, where Z is the sample depth in meters, and ΔT is the respective

https://doi.org/10.5194/essd-2026-416
Preprint. Discussion started: 23 June 2026

Open Access Earth System Science Data Discussions

337 difference relative to "Challenger" data in degrees Celsius. Corrections were applied to all temperature profiles from
338 "Gazelle" and "Tuscarora". **Fig. S7** shows distribution of temperature anomalies versus depth for quality-controlled and
339 adjusted "Challenger", "Gazelle", and "Tuscarora" temperature profiles.
340

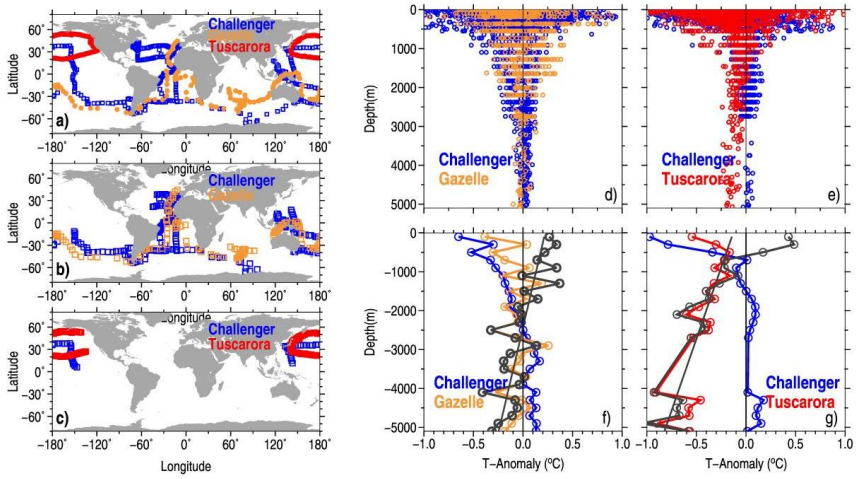

341 **Figure 13. a) Station locations for "Challenger", "Gazelle", and "Tuscarora" expeditions; b) location of "Challenger"**
342 **and "Gazelle"stations used for data inter-comparisons; c) same as b) but for "Challenger" and "Tuscarora" data; d)**
343 **comparison of temperature anomalies for "Challenger" and "Gazelle" data; e) same as d) but for "Challenger" and**
344 **"Tuscarora" data; f) mean temperature anomalies in 200-meter layers for "Challenger"(blue) and "Gazelle" (orange) data**
345 **and the respective anomaly difference (black); same as f) but for "Challenger" blue) and "Tuscarora" (red) data.**
346

347 ## 8. Secular changes of the ocean thermal state since 1870s based on in-situ observations
348

349 ### 8.1 Calculation of temperature anomalies

350 Because of a sparse sampling we estimate the mean thermal state of the entire global ocean and of the main three
351 oceans for 5-25 year long time periods, rather than for distinct calendar years. The earliest time period spans the quasi-
352 global oceanographic survey conducted by "Challenger", "Gazelle", and "Tuscarora". The following time periods are
353 selected: 1873-1877, 1920-1944, 1945-1969, 1970-1989, 1990-2009, 2010-2025. For the calculation of temperature
354 anomalies we use profiles interpolated on 10-meter levels and described in Section 4. For each time period mean
355 anomalies are calculated for 5° × 5° Latitude/Longitude boxes.
356

357 ### 8.2 Spatial patterns of temperature anomalies

358 Difference anomaly maps (**Fig. 14**) illustrate temperature changes between the respective time periods in the layers
359 0-500 m, 500-1000 m, 1000-1500 m, and 1500-2000 m. During the two earliest periods 1873-1877 and 1920-1944,
360 large areas in the central parts of the Pacific and Indian oceans remained essentially unsampled, and no time trends can
361 be calculated (**Fig. 14a, f, k, p**). The general data paucity is also reflected in patchiness of the basin-scale temperature
362 anomaly patterns due to remaining biases and mesoscale noise. However, within each layer a progressive warming
363 between 1870s and 1920s can be seen, with the warming most pronounced in the Atlantic ocean (**Fig. 14a, f, k, p**).
364 Between 1920-44 and 1945-69 (**Fig. 14b, g, l, q**) the maps indicate a strong warming in the tropical and subtropical

https://doi.org/10.5194/essd-2026-416
Preprint. Discussion started: 23 June 2026

latitudes of the Atlantic Ocean for the upper 0-500 m layer and in the northern part of the Atlantic ocean within 1500-2000 m layer. A vast area of cooling is found in the northern part of the Indian ocean. However, the data basis is rather poor in this region.

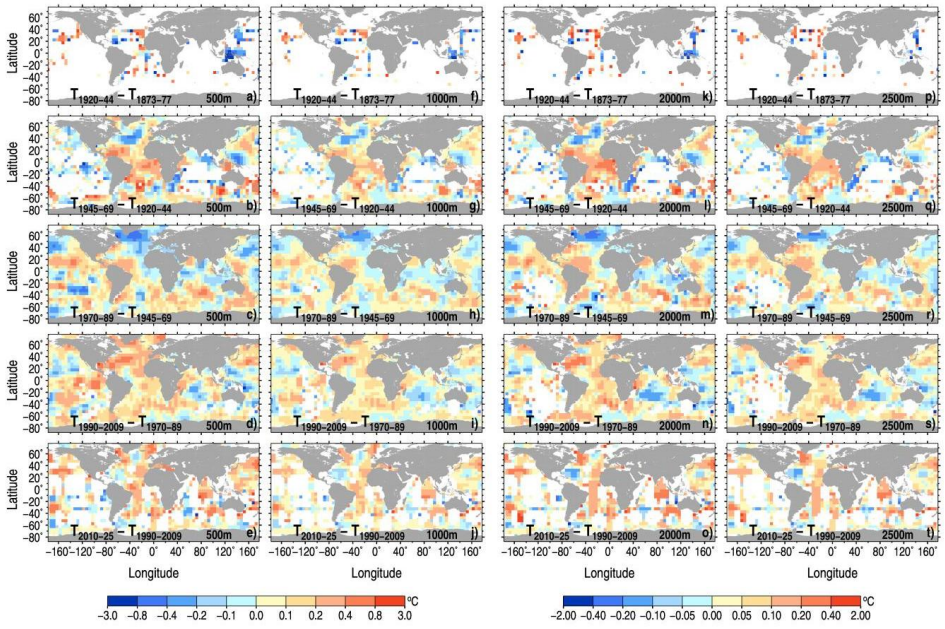

Figure 14. Layer-averaged temperature anomaly differences in 5° × 10° latitude/longitude boxes: 0-500 m (a-e), 500-1000 m (f-j), 1000-1500m (k-o), and 1500-2000 m (p-t).

Between the period 1945-1969 which is strongly biased to the data from the International Geophysical Year 1957-1958 and the most data abundant period 1970-1989 the upper 500 m layer exhibits a global warming pattern except for the North Atlantic and North Pacific oceans (**Fig. 14c**). In the deeper layers the strongest warming is confined to the tropical and subtropical regions of the Atlantic ocean, with a weaker warming in the North Pacific ocean. For the following period between 1970-1989 and 1990-2009 (the latter is dominated by the data from the World Ocean Circulation Experiment) a global warming pattern is found, including the Arctic Ocean, but with the exception for the central Indian ocean and the south-western part of the North Pacific ocean. The prevailing warming trend remains for the deeper layers with the exception (below 1000 m) of the North Atlantic ocean. Also the southern part of the Indian Ocean indicates cooling, most pronounced for the layers 500-1000 m and 1000-1500 m (**Fig. 14i,n**). The progressing global-scale warming within the upper 500 m is revealed for the latest period between 1990-2009 and 2010-2025 (**Fig. 14 e, j, o, t).** For the layer below 500 m the strongest warming is found in the northern and southern part of the Atlantic Ocean. The cooling is confined to the area in the western part of the North Atlantic Ocean between 20-40 N.

8.3 Basin-wide and global vertical profiles of temperature anomalies

Box-averaged temperature anomalies are used to calculate vertical profiles of average anomalies for distinct oceans and for the entire global ocean. As already indicated by the spatial anomaly difference patterns (**Fig. 14**) the

https://doi.org/10.5194/essd-2026-416
Preprint. Discussion started: 23 June 2026

most profound temperature changes took place in the Atlantic Ocean (**Fig. 15a, b**), with Pacific Ocean showing the smallest secular temperature changes (**Fig. 15f**). For the global ocean the continuous warming between 1870s and 2020s is seen throughout the entire water column, except for a close to zero warming between 1945-1969 and 1970-1989 time periods within the upper 500 m (**Fig. 15g, h**). Since 1920s the upper 50 m layer warmed by about 0.65 ºC globally, whereas the global temperature increase at 1000 m and 2000 m level amounts to 0.1ºC and 0.04 ºC respectively.

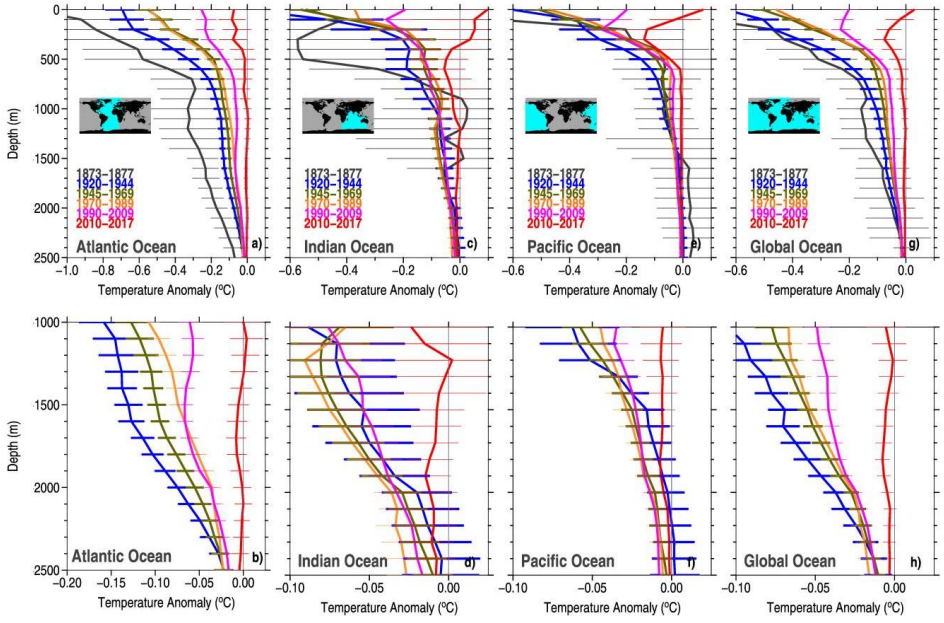

Figure 15. a, c, e, g) Temperature anomaly vertical profiles for the three main oceans and for the entire global ocean and for selected six time periods with standard error bars; b, d, f, h) same but for the depth range below 1000 m.

8.4 Error estimation

The box-averaged temperature anomalies in each 100 m layer are calculated using all observed anomaly profiles within the respective 5° × 5° latitude/longitude box, which are assumed to be independent of each other. The instrumental errors and the mesoscale variability introduce noise which causes error in the estimated box-averaged anomalies. For the basin- and global mean anomalies the errors are obtained by the summation in quadrature of within-box errors. In order to estimate the number of degree of freedom we calculated spatial autocovariances in east-west and north-south directions using box-averaged anomalies for the best sampled periods 1945-1969, 1970-1989, and 1990-2009 (**Fig. S8**). The meridional correlation radius is determined by the zero-crossing and is taken to be 1 meridional distance (555 km) between the boxes. The correlation along longitude has a long tail, so we define the correlation radius as the distance where correlation function falls below 0.1 giving on average two distances between the boxes in zonal direction.

8.5 Secular changes of the Ocean Heat Content

Finally, mean temperature anomaly profiles for three main oceans and for the global ocean were used to calculate OHC time series shown in **Fig. 16** for the layer 0-2000 m**.** The following values of parameters were used for the OHC

https://doi.org/10.5194/essd-2026-416
Preprint. Discussion started: 23 June 2026

calculations: 4184 J/kg°C as the seawater specific heat capacity, 1028 kg/m^3 as the average seawater density, 6371 km as the mean Earth radius. The volumes of the 100 m layers for which temperature anomalies were obtained are calculated using the GEBCO digital bathymetry (Becker et al., 2009). For the earliest time period 1873-1876 the global OHC estimate is represented by the weighted average of the OHC estimates for Atlantic, Indian, and Pacific oceans, with wights equal to individual ocean areas.

Firstly, we note a good agreement between our OHC time series calculated for the selected time periods and the yearly time series of the Institute of Atmospheric Physics (IAP) by Pan et al. (2026) (**Fig. 16a**). There several significant differences between the two products: the Pan et al. (2026) calculations are based on a much larger dataset, which includes not only Nansen casts but all other instrumentation types as well; with the mapping procedure aiming to fill the data-void areas (Cheng and Zhu, 2017).

Secondly, we find that the global ocean undergone a significant warming before 1960 when the IAP and other observation-based time series begin. The median year for the six time periods indicated in the previous section are: 1874.5, 1932.1, 1962.1, 1978.8, 1997.7, and 2015.2. Between 1932 and 1961 the global ocean heat content increased by 149 ZJ to be compared with 456 ZJ warming between 1932 and 2015, thus amounting to 30% of the total OHC increase since 1932. Our calculations further suggest that the warming likely took place also between 1870s and 1920s amounting to 67 ZJ. However, this value is statistically insignificant due to large errors caused by the imperfectness of the earliest data and due to the insufficient spatial sampling between 1873-1877.

OHC time series for the upper 2000 m from Zanna et al. (2018) and Wu et al. (2025) are also compared with our calculations. These time series are based on the reconstruction of the full-depth temperature changes using temperature anomaly at the sea surface as a passive tracer which is carried into the ocean interior via ocean transport processes. Our observation-based time series agree well with the indirectly obtained time series by Zanna et al. (2018) and Wu et al. (2025) indicating a significant OHC increase between 1920s and 1960s.

As discussed above historical Nansen casts are subject to a depth bias (Gouretski et al., 2022). Depth corrections suggested in Table 1 were applied to the original sample depths when they belong to the subset of the following 67 round number and "standard" depth levels:
5, 10, 15, 30, 25, 30, 35, 40, 45, 50, 60, 70, 75, 80, 90, 100, 125, 150, 175, 200, 250, 300, 350, 400, 450, 500, 600, 700, 750, 800, 900, 1000, 1100, 1200, 1250, 1300, 1400, 1500, 1600, 1750, 1800, 1900, 2000, 2100, 2000, 2300, 2400, 2500, 2600, 2700, 2800, 2900, 3000, 3200, 3200, 3300, 3400, 3500, 3600, 3700, 3800, 3900, 4000, 4500, 5000, 5500 meters. These 67 levels represent 1.2 percent of all 1-meter levels between the surface and 5500 m depth. For the time period before 1970, 49.5 % of all observations are reported at the above standard levels. The impact of the depth corrections on global OHC estimates is shown in **Fig. 16a.** We found that the difference between temperature anomalies for original and depth-corrected profiles can amount to 5-10 % of the OHC change depending on the time period. Overall, depth corrections lead to the increase of the warming rate. Applying depth corrections increases the total energy gain between 1930 and 2015 by 12.9 %, from 457 ZJ to 515 ZJ. The respective OHC increase between 1962 and 2015 amounts to 6.8 % from 307 ZJ to 328 ZJ.

The average heating rate between the analyzed six time periods is shown in **Fig. 16b.** Our calculations indicate a heating rate of about 1.2±1.1 ZJ year^{-1} before 1930s . During 1920s and 1960s the heating rate increases to 5.0±0.5 ZJ year^{-1} and is the same as for the period between 1970-1989 and 1990-2009. In agreement with Pan et al. (2026), the fastest OHC growth of 10.5±0.7 ZJ year^{-1} is found for the latest period 1990-2009 to 2010-2025.

https://doi.org/10.5194/essd-2026-416
Preprint. Discussion started: 23 June 2026

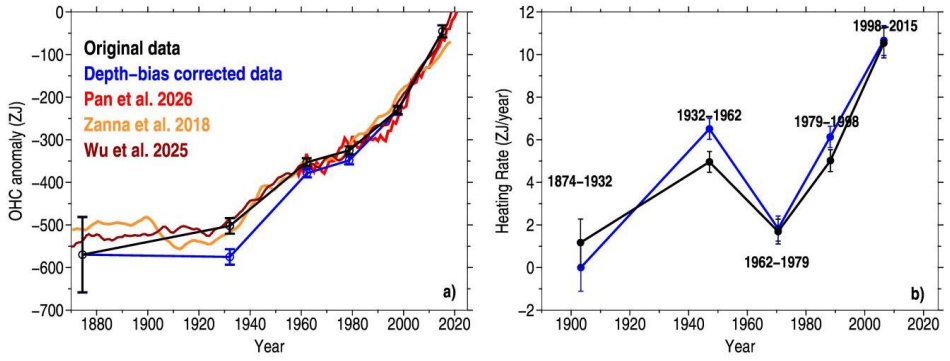

Figure 16. a) OHC anomalies for selected time periods for original data (black) and depth-bias corrected data (blue), OHC anomaly time series from Pan et al. (2026) (red), Zanna et al. (2018) (orange), and Wu et al. (2025) (brown) are shown for comparison; b) heating rate for five time periods in ZJ per year: original profiles (black), depth-bias corrected profiles (blue).

We did not apply corrections for the earliest data from "Challenger", "Gazelle", and "Tuscarora" because a different instrumentation was used on these cruises (a hemp rope instead of a steel one, no bottles attached to the wire). However two arguments are in favor of a positive depth bias in the oldest hydrographic profiles: a) unavoidable deviation of the sounding line from the vertical under real meteorological conditions; b) a significantly larger elasticity of the hemp wire compared to the steel wire, with the Jung's modulus for steel being four time higher compared to hemp. Taking account for possible positive depth bias in the oldest data would result in a positive heating rate between 1870s and 1920s.

9 Discussion and conclusions

The global archive of temperature profiles (Locarnini et al., 2023) was used in a number of studies where the evolution of the thermal state of the global ocean was estimated (Levitus et al., 2005; Gouretski and Koltermann, 2007; Cheng and Zhu, 2016; Pan et al., 2026). However, the entire potential of the historical data archive has not been used as the analyses were based on the data obtained after 1940s. This study takes in focus the oldest subsurface temperature observations, starting with the first subsurface temperature measurements for scientific purposes during the voyage of the British ship "Challenger" in 1870s. Since the old data are less accurate and often provide only a crude vertical resolution a reliable interpolation method is of importance. We applied a combination of the parabolic method by Reiniger and Ross (1966) and the anomaly method by Frankignoul (1981) to the historical profiles to reduce the interpolation error while interpolating over big vertical gaps. All historical profiles undergone a three-step quality control, which includes the statistical quality control automated procedure (Gouretski, 2018), the manual control, and the automated control of temperature anomalies relative to the base-line climatology. The updated WOCE/Argo global hydrographic climatology (Gouretski, 2018) is used, which is based on the high quality temperature profiles for the time period 1990-2025.

Because of the general data paucity we calculated mean temperature anomalies in 5° × 5° latitude/longitude boxes which are used for the estimation of basin-averaged temperature anomalies for 5- to 25-year-long time periods. Our results confirm a progressive warming of the subsurface ocean since 19th century, which is seen both globally and for the three main oceans in all layers above 2000 m. The estimated OHC change since 1950s agrees well with the recent results by Pan et al. (2026), which are based on a much larger dataset and apply a temperature anomaly mapping method (Cheng and Zhu, 2016).

https://doi.org/10.5194/essd-2026-416
Preprint. Discussion started: 23 June 2026

We show that the begin of the ocean warming can be reliably traced back to 1920s and likely even to the end of the 19th century. We find that between 1920-1944 and 1945-1969 the global OHC increased by 139 ZJ. This value amounts to 30 % of the total OHC increase since 1920s.

10 Data availability

The quality control procedure described above was applied to the OSD profiles between 1873 and 2025 from the World Ocean Database and to the additional digitized datasets described in the paper. The resulting dataset comprises observed level data with quality flags and data interpolated on 10-meter levels. The data are in NetCDF and ASCII format and also include the metadata information. The complete dataset (Gouretski et al., 2026) can be found at http://dx.doi.org/10.12157/IOCAS.20260520.001 (Please use email to register and login to access the data.).

Author contributions.

VG and LC – conceptualization, methodology, writing; JD – software, editing, data formatting

Competing interests. The contact author has declared that none of the authors has any competing interests.

Acknowledgments. We thank the National Large Scientific and Technological Infrastructure "Earth System Numerical Simulation Facility" (https://cstr.cn/31134.02.EL) for the technical support. We are thankful to Yuying Pan and Laure Zanna who provided their OHC time series.

Financial support. This study is supported by National Natural Science Foundation of China (Grant no. 42261134536), National Key R&D Program of China (Grant No. 2023YFF0806500), the International Partnership Program of the Chinese Academy of Sciences (Grant No. 060GJHZ2024064MI), Asian Cooperation Fund, the New Cornerstone Science Foundation through the XPLORER PRIZE.

References

Austin, J. F. and McConnel, A.: James Six F. R. S.:- Two hundred years of the Six's self-registering thermometer, Notes Rec R Soc Lond (1980) 35 (1): 49–65, 1980.

Belknap, G. E.: Deep Sea Soundings in the North Pacific Ocean obtained in the United States Steamer Tuscarora, Kessinger Publishing, 90p., 1874.

Becker, J. J., Sandwell, D. T. , F. Smith,W. H., Braud,J. , Binder, B., Depner, J., Fabre, D., Factor, J., Ingalls, S., Kim, S-H., Ladner, R., Marks, K., Nelson, S., Pharaoh, A., Trimmer, R., Von Rosenberg, J., Wallace, G., and Weatherall, P.: Global bathymetry and elevation data at 30 arcsec resolution: SRTM30_PLUS, Marine Geodesy, 32, 4, 355-371, 2009.

Borishanski, L.S.: Manual for the performance of work on standard hydrological sections and marine hydrological surveys, Leningrad, Gydrometeoizdat, 284 p., 1954 (in Russian).

Brennecke, W.: Die ozeanographischen Arbeiten der Deutschen Antarktischen Expedition 1911-1912. Archiv der Deutschen Seewarte, 1921,XXXIX No 1, Hamburg, 1921.

Chapman, S.:The International Geophysical Year, 1957-58, Nature, **175**, 55–56, 1959.

https://doi.org/10.5194/essd-2026-416
Preprint. Discussion started: 23 June 2026

519 Cheng L. and Zhu, J.: Benefits of CMIP5 Multimodel Ensemble in Reconstructing Historical Ocean Subsurface
520 Temperature Variation, Journal of Climate, 29, 5393 – 5415. DOI: 10.1175/JCLI-D-15-0730.1, 2016.
521 Cheng, L. J., and Coauthors: Record high temperatures in the ocean in 2024. Adv. Atmos. Sci., 42, 1092−1109,
522 https://doi.org/10.1007/s00376-025-4541-3, 2025.
523 Frankignoul, C., 1981: On the depth interpolation of repeated hydrographic data, J. Geophys. Res., 86, C3, 2001-2004.
524 Garcia H. E., Boyer, T. P., Baranova, O. K., Locarnini, R. A., Mishonov, A. V., Grodsky, A. , Paver, C. R., Weathers,
525 K. W. Smolyar, I.V., Reagan, J. R., Seidov, D., Zweng, M. M.: World Ocean Atlas (2018): Product
526 Documentation. A. Mishonov, Technical Editor, 2019.
527 Gebbie, G. and Huybers , P.: The littele ice age and 20th-century deep Pacific cooling. Science, 363, 70-74, 2019.
528 Gould, J., Sloyan, B., and Visbeck, M.: Chapter 3 - In Situ Ocean Observations: A Brief History, Present Status,
529 and Future Directions, International Geophysics, 103, 59-81, https://doi.org/10.1016/B978-0-12-391851-
530 2.00003-9, 2013.
531 Gouretski, V. and Koltermann, K. P.: How much is the ocean really warming? Geophys. Res. Lett., 34, L01610,
532 doi:10.1029/2006GL027834, 2007.
533 Gouretski, V., Jungclaus, J. H., and Haack, H. : Revisiting the Meteor 1925–1927 hydrographic dataset reveals
534 centennial full-depth changes in the Atlantic Ocean, Geoph. Res. Letters, 40, 10, 2236-2241,
535 https://doi.org/10.1002/grl.50503, 2012.
536 Gouretski, V.: World Ocean Circulation Experiment – Argo Global Hydrographic Climatology. Ocean Science, 14,
537 1127-1146, 2018.
538 Gouretski, V. and Cheng, L.: Correction for Systematic Errors in the Global Dataset of Temperature Profiles from
539 Mechanical Bathythermographs, Journal of Atmospheric and Oceanic Technology, 37, 5, 841-
540 855, 10.1175/JTECH-D-19-0205.1, 2020.
541 Gouretski, V., Cheng, L., and Boyer, T. On the Consistency of the Bottle and CTD Profile Data. J. Atmos. Oceanic
542 Technol., 39, 1869–1887, https://doi.org/10.1175/JTECH-D-22-0004.1, 2022.
543 Gouretski, V., Cheng, L., Du, J., Xing, X., Chai, F., and Tan, Z.: A consistent ocean oxygen profile dataset with new
544 quality control and bias assessment, Earth Syst. Sci. Data, 16, 5503–5530,
545 https://doi.org/10.5194/essd-16-5503-2024, 2024.
546 Gouretski, V., Cheng, L., and Du, J.: IAP Historical Nansen Cast Temperature Profile Dataset[data set], Marine Science
547 Data Center, Chinese Academy of Sciences (https://msdc.qdio.ac.cn), doi:10.12157/IOCAS.20260520.001, 2026.
548 Helland-Hansen, B., and Nansen, F.: The Norwegian Sea: Its Physical Oceanography Based upon the Norwegian
549 Researches 1900–1904. Vol. II. Det Mallingske Bogtrykkeri, 390pp., 1909.
550 Hydrographisches Amt der Admiralität: Forschungsreise S.M.S. “Gazelle” in den Jahren 1874 bis 1876, II. Theil,
551 Physik und Chemie, 1888.
552 Levitus, S., Antonov, J., and Boyer, T.: Warming of heworld ocean, 1955-2003, Geophysical Research Letters, 32,
553 L02604, doi:10.1029/2004G, 2005.
554 Locarnini, R. A., Mishonov, A. V., Baranova, O. K., Reagan, J. R., Boyer, T. P., Seidov, D.,Wang, Z., Garcia, H. E.,
555 Bouchard, C., Cross, S.L., Paver, C. R., and Dukhovskoy, D.: World Ocean Atlas 2023, Volume 1:
556 Temperature. A. Mishonov Technical Ed. NOAA Atlas NESDIS 89, doi.org/10.25923/54bh-1613, 2024.
557 Moroshkin, K.V.: Experience of work with domestic unprotected thermometers, Collectedworks of the Institute of
558 Oceanology, Academy of Sciences of the USSR, 5, 78, 92, 1951 (in Russian).

https://doi.org/10.5194/essd-2026-416
Preprint. Discussion started: 23 June 2026

559 Nansen, F.: The Norwegian North Polar Expedition, 1893–1896, Scientific Results, edited by Fridtjof Nansen, Volume
560 VI, London, 659 p., 1905.
561 Negretti, H. and Zambra, J. W.: On new deep-sea thermometer. Proc. R. Soc. (1874) 22 (148-155): 238–241, 1874.
562 Pan, Y. Y., and Coauthors: Ocean heat content sets another record in 2025, Adv. Atmos. Sci.,
563 https://doi.org/10.1007/s00376-026-5876-0, 2026.
564 Rayner N. A , Parker, D. E., Horton, E. B., Folland, C. K., Alexander, L. V., Rowell, D. P., Kent, E. C., Kaplan, A.:
565 Global analyses of sea surface temperature, sea ice, and night marine air temperature since the late nineteenth
566 century, Journal of Geoph. Res., 108, D14, 4407, DOI: https://doi.org/10.1029/2002JD002670, 2003.
567 Reiniger, R.F. and Ross, C.K.: A method of interpolation with application to oceanographic data, Deep-Sea Res.,
568 15,2,185-193, 1968.
569 Roemmich, D., Gould, W. J., and Gilson, J.: 135 years of global ocean warming between the Challenger expedition and
570 the Argo Programme. Nature Clim Change, **2**, 425–428, https://doi.org/10.1038/nclimate1461, 2012.
571 Spilhaus, A. F.: A bathythermograph. Journal of Marine Research 1, (2),
572 https://elischolar.library.yale.edu/journal_of_marine_research/522, 1938.
573 State Oceanographic Institute: Manual fort hydrological works in oceans and seas, second edition, Leningrad,
574 Gidrometeoizdat, 725 p, 1977.
575 Thomson, W. and Murray, J.: The Voyage of H.M.S. Challenger 1873-1876. Narrative, Vol.1, First Part, Ch. III, ed.
576 Johnson Reprint Corporation, available at http://archimer.ifremer.fr/doc/00000/4751/, 1885.
577 Thomson, C. W. and Murray, J.: Report on the Scientific Results of the Voyage of H.M.S. Challenger during the years
578 1873-76, Pysics and Chemistry, Vol. II, Her Majesty Stationary Office, London, 1889.
579 U.S. Hydrographic Office: Deep-Sea Soundings in the North Pacific Ocean obtained in the United States Steamer
580 Tuscarora, Commander George E. Belknap, Washington, Government Printing Office, 1874.
581 U.S. Naval Oceanographic Office: Instruction manual for obtaining oceanographic data, Washigton D.C., U.S.
582 Government Printing Office, 232 p., 1968.
583 Wu, Q., Gregory, G. M., Zanna, L., and Khatwala, S.: Time-varying global energy budget since 1880 from a
584 reconstruction of ocean warming, Earth, Atmospheric, and Planetary Sciences, 122, 20,
585 https://doi.org/10.1073/pnas.2408839122, 2025.
586 Wunsch, C. and Heimbach, P.: Practical global oceanic state estimation. Physica D, 230, 197-208,
587 doi:10.1016/j.physd.2006.09.040, 2007.
588 Wüst, G., Böhnecke, G., and Meyer, H. F.: Ozeanographische Methoden und Instrumente, in: Wissenschaftliche
589 Ergebnisse der Deutschen Atlantischen Expedition auf dem Forschungs und Vermessungsschiff “Meteor” 1925–
590 1927, Band IV, Erster Teil (ed. von Walter de Gruyter &CO.), Berlin, 1932.
591 Zanna, L., Khatiwaia, S., Gregory, J.M., Ison, J., and Heimbach, P.: Global reconstruction of historical ocean heat
592 storage and transport, Proceedings of the National Academy of Sciences 116(4), DOI:10.1073/pnas.180883811521,
593 2019.

https://doi.org/10.5194/essd-2026-416
Preprint. Discussion started: 23 June 2026

Open Access Earth System Science Data Discussions

Appendix A: Corrections for depth bias

Table A1. Depth corrections for historical Nansen casts

Original Depth	Correction factor
0050	0.9400
0100	0.9600
0200	0.9750
0250	0.9800
0300	0.9833
0400	0.9835
0500	0.9840
0600	0.9845
0800	0.9860
1000	0.9880
1200	0.9885
1500	0.9900
2000	0.9900
2500	0.9900
3000	0.9900
3500	0.9900
4000	0.9937
4500	0.9937
5000	0.9937